The ICRP recommended methods of red bone marrow dosimetry

Maria Zankl [a,*], Jonathan Eakins [b], José-María Gómez Ros [c], Christelle Huet [d]

[a] Helmholtz Zentrum München (GmbH) German Research Center for Environmental Health, Institute of Radiation Medicine, Ingolstädter Landstr. 1, 85764 Neuherberg, Germany
[b] Public Health England CRCE, Chilton, UK
[c] CIEMAT – Centro de Investigaciones Energéticas, Medioambientales y Tecnológicas, Madrid, Spain
[d] Institut de Radioprotection et de Sûreté Nucléaire, Fontenay-aux-Roses, France

ABSTRACT

To account for an enhancement of the absorbed dose to both active marrow and endosteum due to secondary electrons generated in bone trabeculae and depositing energy in adjacent marrow tissues, a specific method for bone dosimetry has been developed and introduced in ICRP Publication 116 for photons and neutrons. In a recent intercomparison exercise on the usage of the ICRP/ICRU adult reference computational phantoms carried out by EURADOS WG6, it turned out that many participants found it difficult to correctly apply the bone dosimetry method as recommended by the ICRP. The purpose of this article is, therefore, to provide practical guidance and technical hints for incorporating the ICRP bone dosimetry method into various types of radiation transport codes.

1. Introduction

EURADOS, the European Radiation Dosimetry Group, is a network of more than 75 European institutions and 600 scientists coordinated in working groups that – among other activities – organises scientific meetings and training activities as well as intercomparison and benchmark studies.

EURADOS Working Group 6 "Computational Dosimetry" recently organised an intercomparison study (Zankl et al., 2021) on the usage of the ICRP/ICRU adult reference computational phantoms (ICRP, 2009) that aimed to investigate whether the phantoms have been correctly combined with the radiation transport codes used, and if the participants are able to correctly apply ICRP guidance on the evaluation of such specific quantities as dose to the red bone marrow (ICRP, 2010) and effective dose (ICRP, 2007).

The skeleton is mainly composed of cortical bone, trabecular bone, active (red) and inactive (yellow) bone marrow, and cartilage. For purposes of radiological protection, the ICRP defines two skeletal cell populations of dosimetric interest relevant to stochastic biological effects: (1) haematopoietic stem cells associated with the risk of radiogenic leukaemia, and (2) osteoprogenitor cells associated with the risk of radiogenic bone cancer. Current modelling for radiological protection assumes the former cells to be uniformly distributed within the marrow cavities of haematopoietically active marrow, i.e., the red bone marrow. In ICRP Publication 110 (ICRP, 2009), the surrogate target tissue for the osteoprogenitor cells was defined as being 50 μm in thickness along the surfaces of the bone trabeculae in skeletal spongiosa, and along the inner surfaces of the medullary cavities in the shafts of all long bones. Due to encompassing the total marrow (active and inactive) within 50 μm distance from the bone surfaces, the symbol chosen for this target region is TM_{50}.

The dimensions of internal structures of these tissues are of the order of micrometres and therefore much smaller than the resolution of a normal CT (computed tomography) scan (order of millimetres). Thus, these volumes could not be 'segmented' in the reference computational phantoms, i.e. resolved into separate voxelised regions. Instead, an alternative scheme had to be developed in order to represent the gross spatial distributions of the various bone tissues as realistically as possible for the given voxel resolution (Zankl et al., 2007). For this purpose, the skeleton was divided into those nineteen bones and bone groups for which individual data on red bone marrow content and marrow cellularity are given in ICRP Publication 70 (ICRP, 1995). These bones are: upper halves of humeri, lower halves of humeri, lower arm bones (ulnae and radii), wrists and hand bones, clavicles, cranium, upper halves of femora, lower halves of femora, lower leg bones (tibiae, fibulae and patellae), ankles and foot bones, mandible, pelvis (os coxae),

ribs, scapulae, cervical spine, thoracic spine, lumbar spine, sacrum, and sternum. These were then sub-segmented into an outer shell of cortical bone and the enclosed spongiosa part of the bone. The long bones contain a medullary cavity as a third component, which is enclosed by cortical bone. This sub-division resulted in 44 different 'identification numbers' (i.e. distinct tissue regions) in the skeleton: two – cortical bone and spongiosa – for each of the nineteen bones mentioned above, and a medullary cavity for each of the six long bones (upper and lower half of humeri, lower arm bones, upper and lower half of femora, and lower leg bones). Furthermore, the amount of cartilage that could be identified on the CT images and could, thus, be segmented directly, was attributed to four body parts – head, trunk, arms and legs. Hence, the skeleton covers a total of 48 individual identification numbers.

For each bone (group), the spongiosa region encompasses red (or active) bone marrow, yellow (or inactive) bone marrow, and trabecular bone. The reference values of the total amount of red marrow and its percentage distribution among individual bones as given in ICRP Publications 70 and 89 (ICRP, 1995, 2002), based on earlier data of Cristy (1981), permit evaluation of the amount of red bone marrow in each bone (group). Furthermore, the bone marrow cellularity (Cristy, 1981; ICRP, 1995) in an individual bone, i.e. the red bone marrow fraction, permits the evaluation of the volume of yellow marrow from the red bone marrow volume. The remaining spongiosa volume of each bone is then assigned to trabecular bone. Accordingly, each of the nineteen bones or bone groups has its own unique bone-specific spongiosa composition. The elemental composition of endosteum is equal to that of the active marrow/inactive marrow mixture in a particular skeletal site, as determined by its reference marrow cellularity (ICRP, 1995).

Fig. 1 shows the fine structure of trabecular bone (from https://en.wikipedia.org/wiki/Trabecula) and how the spongiosa volume of each bone is composed of trabecular bone, red and yellow bone marrow. The scale of these structures (~tens of μm) in Fig. 1 (*left*) is orders of magnitude lower than the resolution of the voxel phantoms (~few mm), which are therefore forced to adopt a homogenized approach to bone spongiosa. This approach is illustrated in Fig. 1 (*right*), where the red and yellow bone marrow and trabeculae are incorporated into a single, uniform tissue composition. The proportional contributions of these constituents vary between the spongiosa of different bones.

For higher-energy directly ionising radiations, mean spongiosa doses are reasonable approximations for doses to active marrow and endosteum. For indirectly ionising radiations such as photons and neutrons, there are energy ranges in which secondary charged-particle equilibrium does not exist across the marrow cavities. During photon irradiation of spongiosa at energies below ~200 keV, a greater number of photo-electric events occur in bone trabeculae than in the comparatively less dense marrow tissues. As a result, the absorbed dose to both active marrow and endosteum is enhanced due to secondary electrons that are generated in bone trabeculae and deposit energy in adjacent marrow tissues (Johnson et al., 2011). The dose enhancement to endosteum is more pronounced than that to active marrow because of its smaller 50 μm thickness and closer proximity to the bone trabeculae surfaces. For neutrons at energies below ~150 MeV, on the other hand, elastic and inelastic collisions in spongiosa result in a greater number of recoil protons born in the marrow tissues than in the bone trabeculae, due to the higher hydrogen content of marrow, and many of these recoil particles traverse the marrow spaces with their residual energy being lost to surrounding trabeculae. The net result for neutron irradiation over large energy ranges is then a suppression of the absorbed dose to marrow tissues in comparison with that predicted by assuming a kerma approximation (Bahadori et al., 2011; Kerr and Eckerman, 1985).

To account for these effects, a specific method for bone dosimetry has been developed and introduced in ICRP Publication 116 (ICRP, 2010), based on bone- and energy-specific fluence-to-dose response functions for photons and neutrons.

One of the more general findings of the EURADOS Intercomparsion Exercise was that several participants had problems in correctly utilising the ICRP-recommended bone dosimetry method in their practical applications (Zankl et al., 2021). The purpose of this article is, therefore, to provide practical guidance and technical hints for incorporating the ICRP bone dosimetry method into various types of radiation transport codes.

2. The bone dosimetry method recommended by ICRP Publication 116

This section closely follows the explanations of ICRP Publication 116 (ICRP, 2010), specifically those given in Section 3.4 (electrons), Annex D (photons), and Annex E (neutrons)

2.1. Electrons

For electrons, the energy deposition within a specific spongiosa site is assumed to occur uniformly, so that the dose to all spongiosa constituents – active/inactive marrow, endosteum and trabecular bone – is approximately constant throughout the entire spongiosa site. This means that the dose to active marrow, as well as the dose to endosteum, in a specific bone can be approximated by the dose to the entire spongiosa of this bone:

$$D(r_T, x) = D(SP, x) \tag{1}$$

where $D(r_T, x)$ is the dose to 'target' region r_T in bone site x, with r_T either active marrow, AM, or endosteum, TM_{50}, $D(SP, x)$ is the mean
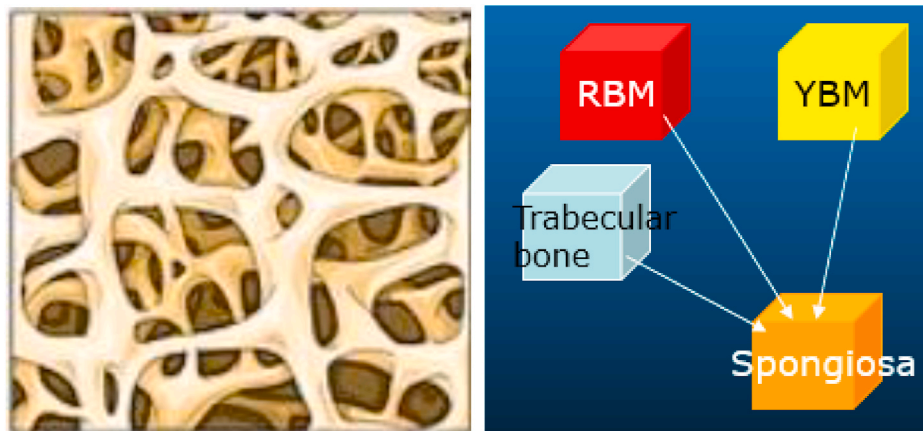
Fig. 1. Left: microscopic structure of trabecular bone (from https://en.wikipedia.org/wiki/Trabecula); right: three components making up the spongiosa composition.

dose to spongiosa of bone site x, and x is one of the 19 distinct bones and bone groups defined within the skeleton.

As already mentioned above, the composition of each spongiosa site has bone-specific relative amounts of active/inactive marrow, endosteum and trabecular bone and, hence, a specific elemental composition. Therefore, it is necessary to evaluate the radiation transport and the energy depositions in each spongiosa site separately. The dose to the target regions in the whole skeleton is then evaluated as a mass-averaged dose to the spongiosa-site specific target region doses:

$$D_{skel}(AM) = \sum_x \frac{m(AM,x)}{m(AM)} D(SP,x) \tag{2}$$

where $D_{skel}(AM)$ is the dose to active marrow in the entire skeleton, $m(AM,x)$ is the active marrow mass in bone site x, and $m(AM)$ is the mass of active marrow in the entire skeleton. For the endosteum, there is an additional contribution from the medullary cavities in the shafts of the long bones:

$$D_{skel}(TM_{50}) = \sum_x \frac{m(TM_{50},x)}{m(TM_{50})} D(SP,x) + \sum_x \frac{m(TM_{50},x)}{m(TM_{50})} D(MM,x) \tag{3}$$

where $D_{skel}(TM_{50})$ is the dose to endosteum in the entire skeleton, $m(TM_{50},x)$ is the endosteum mass in bone site x, $m(TM_{50})$ is the endosteum mass in the entire skeleton, and $D(MM,x)$ is the dose to the medullary marrow in bone site x.

For active marrow, there is no dose contribution from the medullary cavities in the shafts of the long bones, since these do not contain active marrow in the adult reference computational phantoms.

The masses of active/inactive marrow and endosteum of all 19 bones and bone groups are given in Table 4.2 of ICRP Publication 110 (ICRP, 2009), and the elemental compositions of all spongiosa sites are given in Tables B.1 and B.2 of that same ICRP Publication.

2.2. Photons

For photons, secondary particle equilibrium between the marrow cavities and bone trabeculae is established for energies above approximately 200 keV, because the ranges of those secondary electrons have become sufficiently long compared to the scales of the micro-structures within the bones (ICRU, 1984). Below that energy, the absorbed dose to both active marrow and endosteum is enhanced due to secondary electrons that are generated in bone trabeculae and deposit energy in adjacent marrow tissues (Johnson et al., 2011). The dose enhancement to endosteum is more pronounced than that to active marrow because of its smaller 50 μm thickness and closer proximity to the bone trabeculae surfaces. To account for this increased dose, several groups have established so-called "response functions" $R(r_T \leftarrow r_S, x, E)$ that represent the absorbed dose to the target tissue per photon fluence (Eckerman, 1985; Eckerman et al., 2007; Hough et al., 2011; Johnson et al., 2011). The parameters are as follows: x is the index for the various bone sites, where for the long bones spongiosa and medullary cavities are considered as two separate bone sites; r_T is the index for the target region for dose assessment (active marrow or endosteum); r_S is the index for the source region in bone site x (spongiosa or medullary marrow) where the fluence is scored; and E is the energy of the photon passing through and potentially interacting within skeletal region r_S of bone site x. The response functions of ICRP Publication 116 have been established by researchers at the University of Florida (Hough et al., 2011; Johnson et al., 2011).

The absorbed dose to tissue r_T in bone site x is then determined as the integral over all energies of the bone-specific energy dependent photon fluence and the bone-specific energy dependent dose response function:

$$D(r_T, x) = \int_E \Phi(E, r_S, x) R(r_T \leftarrow r_S, x, E) dE \tag{4}$$

where $D(r_T, x)$ is the absorbed dose to tissue r_T in bone site x, $\Phi(E, r_S, x)$ is the energy dependent photon fluence through source region r_S in bone site x, and $R(r_T \leftarrow r_S, x, E)$ is the bone-specific energy dependent dose response function.

For photons, there is also an alternative method to account for the lack of secondary electron equilibrium between the spongiosa constituents and the resulting increase in active marrow and endosteum doses below 200 keV. Instead of applying dose response functions to energy-dependent fluence, scaling factors to spongiosa kerma can be applied alternatively (Kramer, 1979; Lee et al., 2006; Schlattl et al., 2007; Zankl et al., 2002). This approach, where the absorbed dose to active marrow and endosteum is determined by applying three factors to the kerma to spongiosa or medullary marrow, is sometimes also called "three-factor method". The approach is as follows:

$$D(AM,x) = \int_E K(SP,x,E) \left[\frac{\mu_{en}}{\rho}(E) \right]_{SP}^{AM} S(AM,x,E) dE \tag{5}$$

and

$$D(TM_{50},x) = \int_E K(SP/MM,x,E) \left[\frac{\mu_{en}}{\rho}(E) \right]_{SP/MM}^{TM} S(TM_{50},x,E) dE \tag{6}$$

where $K(SP/MM,x,E)$ is the kerma to spongiosa (SP) or medullary marrow (MM) in bone site x contributed by photons of energy E, $\left[\frac{\mu_{en}}{\rho}(E) \right]_{SP}^{AM}$ is the mass energy absorption coefficient (MEAC) ratio in active marrow to that in spongiosa, $\left[\frac{\mu_{en}}{\rho}(E) \right]_{SP/MM}^{TM}$ is the MEAC ratio in total marrow to that in spongiosa or medullary marrow, $S(AM,x,E)$ is the dose enhancement factor for active marrow, and $S(TM_{50},x,E)$ is the dose enhancement factor for endosteum.

With appropriate dose enhancement factors, this approach is numerically equivalent to employing dose response functions (Johnson et al., 2011) but extends applicability of the bone dosimetry method to kerma in addition to fluence, thus broadening its practicability for radiation transport codes.

The dose to target region r_T in the entire skeleton is then evaluated by mass-averaging the bone-specific target region doses,

$$D_{skel}(r_T) = \sum_x \frac{m(r_T,x)}{m(r_T)} D(r_T,x) \tag{7}$$

where $D_{skel}(r_T)$ is the dose to target region r_T in the entire skeleton, $m(r_T,x)$ is the mass of target region r_T in bone site x, and $m(r_T)$ is the mass of target region r_T in the entire skeleton. The target region, r_T, is either active marrow, AM, or endosteum, TM_{50}. For active marrow, the sum over all bone sites x encompasses all spongiosa regions; for the endosteum, additionally the medullary cavities in the shafts of the long bones have to be considered.

2.3. Neutrons

In Annex E of ICRP Publication 116 (ICRP, 2010), corresponding dose–response functions for neutron irradiation of the skeletal tissues are presented (Bahadori et al., 2011; Kerr and Eckerman, 1985). These functions are given over the energy range from 10^{-3} eV to 150 MeV. They explicitly consider the transport of recoil protons across both the bone trabeculae and marrow cavities of each skeletal site: in the neutron energy range from 10^{-3} eV to 20 MeV only recoil protons from hydrogen collisions are considered, but protons originating from collisions with all skeletal tissue nuclei are also included for neutron energies from 20 to 150 MeV. Non-proton recoil nuclei are assumed to deposit their energy locally at the site of neutron interaction (i.e. the kerma approximation). Above 150 MeV, the absorbed dose to homogeneous spongiosa was found to be a reasonable estimate of the absorbed dose to both active

marrow and endosteum (ICRP, 2010).

The bone-specific absorbed dose to target tissue r_T in bone site x, $D(r_T, x)$, is determined as the integral of the product of the bone-specific energy-dependent neutron fluence $\Phi(E, r_S, x)$ and the bone-specific energy-dependent dose–response function $R(r_T \leftarrow r_S, x, E)$:

$$D(r_T, x) = \int_E \Phi(E, r_S, x) R(r_T \leftarrow r_S, x, E) dE \qquad (8)$$

It should be noted that E is the energy of the neutron passing through and potentially interacting within skeletal tissues, and not the energy of the neutron incident upon the external surfaces of the computational phantom. This is an important point to emphasise as it is a potential source of confusion in calculations of effective dose, for which conversely it is the energy (and type) of the particle incident upon the external surfaces of the computational phantom that is used to determine the value of the radiation weighting factor, w_R, that needs to be applied (ICRP, 2007).

Similar to the situation for photons, the dose to target region r_T in the entire skeleton is then evaluated by mass-averaging the bone-specific target region doses, see (Eq. (7)) above.

Although improvements have been introduced to the anatomical realism of the human skeleton more recently, especially by the introduction of mesh-type reference phantoms (ICRP, 2020a, b; Kim et al., 2016; Yeom et al., 2013; Yeom et al., 2016), it is not yet possible to represent the internal fine structures of the spongiosa regions, and the bone dosimetry methods recommended in ICRP Publication 116 are still in use also in these improved phantoms.

3. Practical incorporation of the ICRP 116 recommended bone dosimetry method in Monte Carlo codes

3.1. Electrons

For electrons, implementation of bone dosimetry is rather straightforward, since no specific response functions have to be considered. It should be noted, however, that the composition of each spongiosa site has bone-specific relative amounts of active/inactive marrow, endosteum and trabecular bone and, hence, a specific elemental composition. Therefore, it is necessary to evaluate the radiation transport and the energy depositions in each spongiosa site separately. The amount of active marrow and endosteum for each bone site can be found in ICRP Publication 110 (ICRP, 2009) as well as the elemental composition of each spongiosa site.

The dose coefficients in a specific bone site for both active marrow and endosteum are equal to the respective dose coefficient for the spongiosa of the same bone site. The dose coefficient for the target region in the entire skeleton is then evaluated from the bone-specific ones by mass-averaging over all spongiosa sites in the case of active marrow, and including also additionally the medullary cavities in the shafts of the long bones in the case of endosteum.

3.2. Photons

For evaluating the energy-spectral fluence in the bone-specific spongiosa and medullary cavity sites, ICRP Publication 116 (ICRP, 2010) recommends the use of fluence estimators in the Monte Carlo simulation process, such as a "collision density estimator" or a "track length estimator".

A collision density estimator is used to evaluate fluence as

$$\Phi(E, r_S, x) = \frac{N(E, r_S, x)}{\mu(E, r_S, x) V(r_S, x)} \qquad (9)$$

where $V(r_S, x)$ is the volume of source region r_S in bone site x where the fluence is to be tallied, $N(E, r_S, x)$ is the number of photon interactions occurring within this volume at photon energy E, and $\mu(E, r_S, x)$ is the

corresponding linear attenuation coefficient for the medium of source region r_S at photon energy E.

A "track length estimator" is used to evaluate fluence in the form

$$\Phi(E, r_S, x) = \frac{L(E, r_S, x)}{V(r_S, x)} \qquad (10)$$

where $L(E, r_S, x)$ is the total track length of the photon of energy E in the source region r_S in bone site x.

Many Monte Carlo radiation transport code packages provide the possibility to score energy-differential fluence in the volumes of interest by using, e.g., pre-defined "tallies". For evaluating the absorbed dose to active marrow and endosteum in bone site x, it is thus necessary to score and store the energy dependent fluence in spongiosa site or medullary cavity site x, such that it may subsequently be used according to the schemes described earlier. It should be noted that the energy to be considered is that of the photon passing through and potentially interacting within skeletal tissues, and not the energy of the photon incident upon the external surfaces of the computational phantom. After completion of the Monte Carlo calculation, these site-specific fluence spectra may then be post-processed: the fluence per energy E in bone site x has to be multiplied with the appropriate value of the dose-response function $R(r_T \leftarrow r_S, x, E)$ for energy E and bone site x, and these products have to be summed (see Eq. (4)). It is probably easily understood that the energy intervals for scoring the energy-spectral fluence should be chosen such that they agree well with the energy grid for which the response functions are given. For evaluating the absorbed dose to active marrow and endosteum in the whole skeleton, finally, a mass-weighted average of the site-specific absorbed doses has to be calculated (see Eq. (7)).

Alternatively, several Monte Carlo codes provide the user with the possibility to track and manipulate relevant scoring quantities during the Monte Carlo calculation, rather than only after the calculation has been finished, e.g. via a so-called "user code". For example, it may be possible within the user-defined 'input file' of the code to modify an energy-dependent fluence tally with an energy-dependent weighting function, which may be set equal to the dose response function $R(r_T \leftarrow r_S, x, E)$ for a given bone site and tissue. Repeating this process for all fluence tallies for all bone sites then allows implicit determination of the individual RBM and endosteal doses, such that the code will automatically output the desired enhanced results. These separate bone doses would still then need to be summed and mass-averaged during post-processing, however, according to Eq. (7). A further option may be to directly apply the "three factor method", employing energy-dependent MEAC ratios together with energy-dependent dose enhancement factors to all energy depositions in all skeletal sites "on-the-fly" without the necessity of post-processing. In this case, the energy for which the factors have to be selected is the energy of the photon just before the interaction.

3.3. Neutrons

Also for neutrons, the energy-spectral fluence in the bone-specific spongiosa and medullary cavity sites can be evaluated during the Monte Carlo simulation process by establishing a collision density estimator or a track length estimator (see Eqs. (9) and (10)), or scoring energy-differential fluence in the volumes of interest by using pre-defined "tallies" provided by the Monte Carlo radiation transport package.

The procedure is then the same as described above for photons. One method for evaluating the absorbed dose to active marrow and endosteum in bone site x, is to score and store the energy dependent fluence in spongiosa site or medullary cavity site x. After completion of the Monte Carlo calculation, these site-specific fluence spectra may then be post-processed: the fluence per energy E in bone site x has to be multiplied with the appropriate value of the dose response function $R(r_T \leftarrow r_S, x, E)$

for energy E and bone site x, and these products have to be summed (see Eq. (8)). For evaluating the absorbed dose to active marrow and endosteum in the whole skeleton, finally, a mass-weighted average of the site-specific absorbed doses has to be calculated (see Eq. (7)).

Similarly to photons, different Monte Carlo codes may permit different options for tallying and weighting the required energy-dependent fluences or kerma doses in the various bone sites, and thus provide alternative means for achieving the same ends. Also for neutrons, it is important to understand that the energy to be considered is that of the neutron passing through and potentially interacting within skeletal tissues, and not the energy of the neutron incident upon the external surfaces of the computational phantom!

3.4. ICRP 116 conversion coefficients

The citations given in the sections above provide the scientific basis for the bone dosimetry methods recommended by ICRP for electrons, photons and neutrons. For incident charged particles, ICRP Publication 116 (ICRP, 2010) notes that there are no significant mechanisms for dose enhancement or dose depression, and thus skeletal response functions for externally incident particles other than photons and neutrons are not provided in that report. Interestingly, the elaborate bone dosimetry methods for photons and neutrons introduced in ICRP Publication 116 have not been used for evaluation of the conversion coefficients in the skeletal tissues in that report, probably due to time constraints. Instead, for the estimation of absorbed doses in the skeletal tissues, a simplified method of skeletal dosimetry was applied: absorbed dose to active marrow and endosteum were taken conservatively as the absorbed dose to spongiosa in each individual bone site, and skeletal-averaged absorbed doses to these tissues were taken as the mass-weighted average of the regional spongiosa absorbed dose.

The above issue is particularly important within the context of this current Special Issue on intercomparison exercises, because when initially setting-up a voxel phantom calculation, individuals might optimally choose to benchmark their model against reference datasets. Specifically, they might choose to model a standardised geometry, such as exposure to a broad, plane-parallel, monoenergetic field, and compare their resulting organ and effective doses per fluence against the corresponding data given in ICRP 116. However, whilst they could expect agreement within statistical uncertainties for most organs (assuming they had defined their geometry correctly), if they applied the recommended bone dosimetry methods for neutrons or photons they would find discrepancies with the reference data for RBM and endosteal tissue, potentially by up to several tens of percent. Their estimates for effective dose would also diverge, although by considerably less: the tissue weighting factors, w_T, of 0.12 and 0.1 for RBM and endosteum, respectively, would lessen their impacts to some extent.

4. Worked-example

To help illustrate the techniques discussed in this paper, consider the example of a simple photon exposure. Specifically, consider a scenario in which a person is standing centred on a 200 cm radius disk of uniform ground-surface contamination, from which monoenergetic 60 keV photons are emitted isotropically at a rate of 10^6 cm^{-2} s^{-1}; this configuration corresponds to one of the intercomparison exercises described fully in this Special Issue (Eakins et al., 2021) and is shown in Fig. 2. For simplicity in this example, attention is focused on demonstrating how just the RBM dose rate may be obtained for the male phantom. The description will be framed within the context of calculations made using the MCNP family of codes, which is what was used to derive the reference solution in (Eakins et al., 2021) and was also the most widely used by participants during that exercise. However, the overall methodology and flow of information will of course be common to all other Monte Carlo approaches, even if specific technical details and available options may vary slightly from one code to another.

The sequence of steps to determine the RBM dose rate could be as follows:

1. Without loss of generality, consider first the dose to the RBM within, say, the upper femur bones. The collection of voxels within the anthropomorphic phantom that are associated with the spongiosa of these bones, i.e. those voxels with the same corresponding 'identification number' (in this case, organ ID 29), may be grouped together into one object (or 'cell' in MCNP language). Thus, dosimetrically, the upper femur bones in both legs are taken as a single 'target' entity.

2. A photon fluence tally (e.g. MCNP *f4:p*) is defined on the femora cell.
   - If dose enhancement were to be calculated manually after the simulation has finished, this tally would need to be finely binned in order to provide good resolution of the precise fluence-energy distribution through the cell, for subsequent convolution with the dose response function;
   - Alternatively some codes, such as MCNP, are able to apply energy-dependent weighting functions directly to fluence tallies during the simulation (e.g. via user-specified MCNP '*de*' and '*df*' distributions defined in the input file). In such cases, each photon passing through the scoring cell would be multiplied by a value that depends on its energy, with the average aggregated over all particle histories then outputted as a single number at the end of the simulation.

3. In either case, the weighting function to be applied is the absorbed dose per photon fluence histogram for the RBM of the upper femora, which is given in units of Gy m^2 in Table D.1 of ICRP 116. These dose response data are reproduced here in Table 1, where the photon
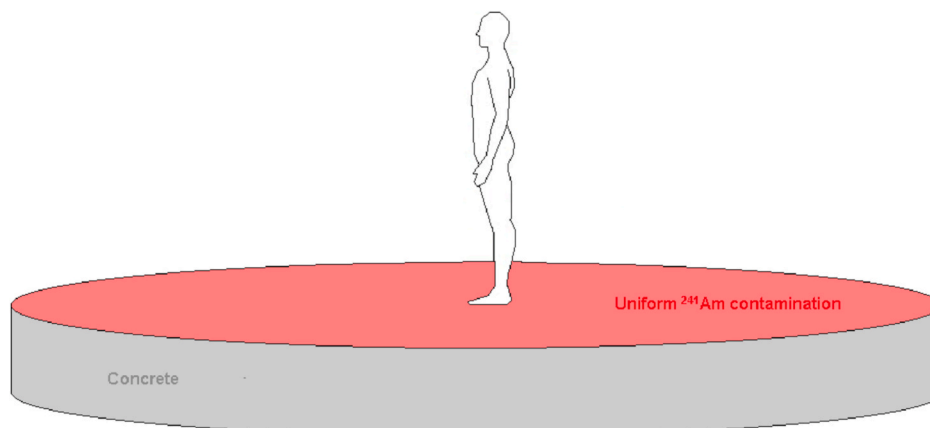
Fig. 2. The phantom standing in vacuum on ground surface-contaminated by Am 241.

Table 1

Absorbed dose per *fluence for the RBM of the spongiosa in the upper femora (organ ID 29), as a function of photon energy.* (Data reproduced from ICRP Publication 116 (ICRP, 2010)).

Energy (MeV)	Dose response (Gy cm^2)	Energy (MeV)	Dose response (Gy cm^2)	Energy (MeV)	Dose response (Gy cm^2)	Energy (MeV)	Dose response (Gy cm^2)
0.01	6.16E-12	0.08	3.28E-13	0.6	3.11E-12	5	1.54E-11
0.015	2.60E-12	0.1	4.08E-13	0.8	4.04E-12	6	1.75E-11
0.02	1.40E-12	0.15	6.63E-13	1	4.90E-12	8	2.17E-11
0.03	6.16E-13	0.2	9.48E-13	1.5	6.72E-12	10	2.60E-11
0.04	3.84E-13	0.3	1.51E-12	2	8.25E-12	–	–
0.05	3.07E-13	0.4	2.07E-12	3	1.09E-11	–	–
0.06	2.89E-13	0.5	2.60E-12	4	1.32E-11	–	–

energies are in MeV and the weighting has been rescaled to Gy cm^2 to match the default cm^{-2} normalization of the MCNP *f4* fluence tally. A linear interpolation scheme is assumed for deriving values at intermediate energies within each bin.

4. For the exercise described in (Eakins et al., 2021), performing these steps provided a result of 5.20×10^{-19} Gy per-source-photon for the dose to the RBM of the upper femora, with that normalization applied by MCNP by default. This quoted reference value was associated with a statistical uncertainty <1%.

5. The above result is then multiplied by the overall mass of RBM in both upper femur bones (i.e. 78.4 g) and then divided by the total mass of RBM in all 13 bone groups of the body in which it is found (i. e. 1170 g), where these masses for the male phantom are given in Table 4.2 of ICRP 110 (ICRP, 2009). The outcome of this calculation is thus the fractional contribution to the whole body RBM dose that arises from the dose to just the upper femora; in this case, it has a value of 3.48×10^{-20} Gy per-source-photon.

6. Steps 1 to 5 are then iterated for the other 12 bone groups that contribute to the overall RBM dose, as specified in Table 4.2 of ICRP 110, i.e. upper humeri, clavicles, cranium, mandible, pelvis, ribs, scapulae, spine (cervical, thoracic and lumbar), sacrum and sternum. Different tallies, dose response functions and masses that are specific to each of these target bones would naturally be required for this task, with those data again tabulated in the ICRP reports.

7. Steps 1 to 6 result in 13 weighted RBM dose components, one from each of the identified bone groups. Summing these individual contributions provides the overall RBM dose to the male from the exposure. In the current example, this summed RBM dose is 2.97×10^{-19} Gy per-source-photon. Note that this value is significantly different from the earlier result for just the upper femora (i.e. 5.20×10^{-19} Gy per-source-photon), which indicates the impact and importance of the weighting method.

8. Lastly, post-processing is typically required to renormalise the Monte Carlo 'per-source-particle' result to something more physically useful. In the present case, multiplication by 1.26×10^{11} ($= \pi \times 200^2 \times 10^6$) accounts for the photon emission rate from the ground contamination, to give the final RBM dose rate value of 3.73×10^{-8} Gy s^{-1} quoted in (Eakins et al., 2021).

A similar sequence of steps would be applied for calculating endosteal doses, noting that 6 further bone targets are required in that iteration to account for additional bone groups and for the medullary cavities of the long bones. Likewise, an analogous process is used for calculating the doses to the bone tissues of the female phantom. Of course, different bespoke dose response functions and bone masses would be required in each case, as detailed in Table D.1 of ICRP 116 and in Table 4.2 of ICRP 110, respectively. Note, however, that the tabulated absorbed dose per fluence data for a given bone are the same for both sexes.

Finally, it is remarked that if the exposure scenario were extended to a mixed radiation field, duplicate tallies would need to be defined on the various bone groups to record the doses from each of the particle species. In particular, if neutrons were present the dose response functions given in Table E.1 of ICRP 116 (ICRP, 2010) would also be required in combination with neutron fluence tallies (e.g. MCNP *f4:n*), in addition to those already used to determine the photon doses. The same iterative processes would still be followed overall, however, with just an extra step '9.' required at the end to appropriately sum the separate field components.

5. Conclusions

EURADOS Working Group 6 "Computational Dosimetry" has organised an intercomparison study (Zankl et al., 2021) on the usage of the ICRP/ICRU adult reference computational phantoms (ICRP, 2009) that aimed to investigate whether the phantoms have been correctly combined with the radiation transport codes used, and if the participants are able to correctly apply ICRP guidance on the evaluation of such specific quantities as dose to the red bone marrow (ICRP, 2010) and effective dose (ICRP, 2007).

For purposes of radiological protection, the ICRP defines two skeletal cell populations of dosimetric interest relevant to stochastic biological effects: (1) haematopoietic stem cells associated with the risk of radiogenic leukaemia, and (2) osteoprogenitor cells associated with the risk of radiogenic bone cancer. The dimensions of internal structures of these tissues are of the order of micrometres and therefore much smaller than the resolution of the reference computational phantoms (order of millimetres) and, thus, these volumes could not be segmented. Instead, alternative schemes have been proposed to represent the gross spatial distribution of the source and target volumes as realistically as possible for the given voxel resolution (Zankl et al., 2007). Active marrow and endosteum are accommodated, together with inactive marrow and trabecular bone, in spongiosa regions with bone-specific compositions that reflect the different relative amounts of these tissues in each bone. For higher-energy directly ionising radiations, mean spongiosa doses are reasonable approximations for doses to active marrow and endosteum. For indirectly ionising radiations such as photons and neutrons, there are energy ranges in which secondary charged-particle equilibrium does not exist across the marrow cavities, and this approximation does not hold. To account for these effects, a specific method for bone dosimetry has been developed and introduced in ICRP Publication 116 (ICRP, 2010), based on bone- and energy-specific fluence-to-dose response functions for photons and neutrons.

One of the more general findings of the EURADOS Intercomparsion Exercise was that several participants had problems in correctly utilising the ICRP-recommended bone dosimetry method in their practical applications. In the present paper, therefore, the necessity of the specific ICRP bone dosimetry method is explained, and the method is described in detail, closely following the explanations of ICRP Publication 116. The use of fluence-to-dose response functions and dose enhancement factors is explained, and practical recommendations are given for implementing the procedures in radiation transport simulations. Thus, it is hoped that these additional explanations and hints may be helpful for the computational dosimetry community to improve the understanding and application of the bone dosimetry methods that are recommended by ICRP.

Declaration of competing interest

The authors declare that they have no known competing financial interests or personal relationships that could have appeared to influence the work reported in this paper.

Acknowledgement

References

Bahadori, A.A., Johnson, P., Jokisch, D.W., Eckerman, K.F., Bolch, W.E., 2011. Response functions for computing absorbed dose to skeletal tissues from neutron irradiation. Phys. Med. Biol. 56 (21), 6873.

Cristy, M., 1981. Active bone marrow distribution as a function of age in humans. Phys. Med. Biol. 26, 389–400.

Eakins, J.S., Huet, C., et al., 2021. Monte Carlo calculation of organ and effective dose rates from ground contamination by 241Am: results of an international intercomparison exercise. Radiat. Meas. Submitted for publication.

Eckerman, K.F., 1985. Aspects of the dosimetry of radionuclides within the skeleton with particular emphasis on the active marrow. In: Schlafke-Stelson, A.T., Watson, E.E. (Eds.), Fourth International Radiopharmaceutical Dosimetry Symposium. Oak Ridge Associates Universities, Oak Ridge, Tennessee, pp. 514–534.

Eckerman, K.F., Bolch, W.E., Zankl, M., Petoussi-Henss, N., 2007. Response functions for computing absorbed dose to skeletal tissues from photon irradiation. Radiat. Protect. Dosim. 127 (1–4), 187–191.

Hough, M., Johnson, P., Rajon, D., Jokisch, D., Lee, C., Bolch, W., 2011. An image-based skeletal dosimetry model for the ICRP reference adult male—internal electron sources. Phys. Med. Biol. 56 (8), 2309–2346.

ICRP, 1995. Basic anatomical and physiological data for use in radiological protection: the skeleton. ICRP Publication 70. Ann. ICRP 25 (2).

ICRP, 2002. Basic anatomical and physiological data for use in radiological protection: reference values. ICRP publication 89. Ann. ICRP 32 (3–4), 5.

ICRP, 2007. The 2007 recommendations of the international Commission on radiological protection. ICRP Publication 103. Ann. ICRP 37 (2–4).

ICRP, 2009. Adult reference computational phantoms. ICRP Publication 110. Ann. ICRP 39 (2).

ICRP, 2010. Conversion coefficients for radiological protection quantities for external radiation exposures. ICRP Publication 116. Ann. ICRP 40 (2–5).

ICRP, 2020. Adult mesh-type reference computational phantoms. In: Sage (Ed.), ICRP Publication 145. International Commission of Radiological Protection.

ICRP, 2020. Paediatric reference computational phantoms. ICRP Publication 143. Ann. ICRP 49 (1).

ICRU, 1984. Stopping Powers for Electrons and Positrons, ICRU Report 37. International Commission on Radiation Units and Measurements, Bethesda, MD.

Johnson, P.B., Bahadori, A.A., Eckerman, K.F., Lee, C., Bolch, W.E., 2011. Response functions for computing absorbed dose to skeletal tissues from photon irradiation – an update. Phys. Med. Biol. 56 (8), 2347–2365.

Kerr, G.D., Eckerman, K.F., 1985. Neutron and photon fluence-to-dose conversion factors for active marrow of the skeleton. In: Schraube, H., et al. (Eds.), Fifth Symposium on Neutron Dosimetry. Commission of the European Communities, Luxembourg, pp. 133–145.

Kim, C.H., Yeom, Y.S., Nguyen, T.T., Wang, Z.J., Kim, H.S., Han, M.C., Lee, J.K., Zankl, M., Petoussi-Henß, N., Bolch, W.E., Lee, C., Chung, B.S., 2016. The reference phantoms: voxel vs polygon. Ann. ICRP 45, 188–201.

Kramer, R., 1979. Ermittlung von Konversionsfaktoren zwischen Körperdosen und relevanten Strahlungskenngrößen bei externer Röntgen- und Gamma-Bestrahlung. GSF - National Research Center for Environment and Health, Neuherberg, Germany.

Lee, C., Lee, C., Shah, A.P., Bolch, W.E., 2006. An assessment of bone marrow and bone endosteum dosimetry methods for photon sources. Phys. Med. Biol. 51 (21), 5391–5407.

Schlattl, H., Zankl, M., Petoussi-Henss, N., 2007. Organ dose conversion coefficients for voxel models of the reference male and female from idealized photon exposures. Phys. Med. Biol. 52, 2123–2145.

Yeom, Y.S., Han, M.C., Kim, C.H., Jeong, J.H., 2013. Conversion of ICRP male reference phantom to polygon-surface phantom. Phys. Med. Biol. 58 (19), 6985–7007.

Yeom, Y.S., Wang, Z.J., Nguyen, T.T., Kim, H.S., Choi, C., Han, M.C., Kim, C.H., Lee, J.K., Chung, B.S., Zankl, M., Petoussi-Henss, N., Bolch, W.E., Lee, C., 2016. Development of skeletal system for mesh-type ICRP reference adult phantoms. Phys. Med. Biol. 61 (19), 7054–7073.

Zankl, M., Eakins, J., Gómez Ros, J.-M., Huet, C., Jansen, J., Moraleda, M., Reichelt, U., Struelens, L., Vrba, T., 2021. EURADOS intercomparison on the usage of the ICRP/ICRU adult reference computational phantoms. Radiat. Meas. 145, 106596. https://doi.org/10.1016/j.radmeas.2021.106596.

Zankl, M., Eckerman, K.F., Bolch, W.E., 2007. Voxel-based models representing the male and female ICRP reference adult – the skeleton. Radiat. Protect. Dosim. 127 (1–4), 174–186.

Zankl, M., Fill, U., Petoussi-Henss, N., Regulla, D., 2002. Organ dose conversion coefficients for external photon irradiation of male and female voxel models. Phys. Med. Biol. 47 (14), 2367–2385.